View metadata, citation and similar papers at core.ac.uk
brought to you by CORE
provided by RERO DOC Digital Library

Journal of Biomolecular NMR, **24:** 291–300, 2002.
KLUWER/ESCOM
© 2002 *Kluwer Academic Publishers. Printed in the Netherlands.*

TROSY experiment for refinement of backbone ψ and ϕ by simultaneous measurements of cross-correlated relaxation rates and $^{3,4}J_{H\alpha HN}$ coupling constants

Beat Vögeli & Konstantin Pervushin*
Laboratorium für Physikalische Chemie, Swiss Federal Institute of Technology, ETH-Hönggerberg, CH-8093 Zürich, Switzerland

Received 28 May 2002; Accepted 2 October 2002

Key words: coherence transfer optimization, cross-correlated relaxation, E.COSY, scalar couplings, secondary structure of proteins, TROSY

Abstract

The TROSY principle has been introduced into a HNCA experiment, which is designed for measurements of the intraresidual and sequential H^{α}-C^{α}/H^{N}-N dipole/dipole and H^{α}-C^{α}/N dipole/CSA cross-correlated relaxation rates. In addition, the new experiment provides values of the $^{3,4}J_{H\alpha HN}$ coupling constants measured in an E.COSY manner. The conformational restraints for the ψ and ϕ angles are obtained through the use of the cross-correlated relaxation rates together with the Karplus-type dependencies of the coupling constants. Improved signal-to-noise is achieved through preservation of all coherence transfer pathways and application of the TROSY principle. The application of the [^{15}N,^{13}C]-DQ/ZQ-[^{15}N,^{1}H]-TROSY-E.COSY experiment to the 16 kDa apo-form of the *E. coli* Heme Chaperon protein CcmE is described. Overall good agreement is achieved between ψ and ϕ angles measured with the new experiment and the average values determined from an ensemble of 20 NMR conformers.

Abbreviations: TROSY, transverse relaxation-optimized spectroscopy; DD, dipole-dipole coupling; CSA, chemical shift anisotropy; 3D, three-dimensional; ZQ (DQ), zero (double) quantum manifold; CcmE, Cytochrome *c* maturation heme chaperone protein E from *E. Coli*; E.COSY, exclusive correlation spectroscopy.

Introduction

In the pursuit of more precise solution structures of proteins the usual sources of structural constraints based on proton-proton NOE cross-relaxation and scalar coupling constants (Wüthrich, 1986) are effectively complemented by dihedral angle estimates derived from the effects of cross-correlated cross relaxation (Ernst and Ernst, 1994; Vincent et al., 1996; Reif et al., 1997). The main focus of newly developed NMR experiments is the determination of various dihedral angles in proteins by the use of quantum interference between spin Hamiltonians, which describe chemical shift anisotropy and dipolar interactions (Yang et al., 1997, 1998; Yang and Kay, 1998; Pelupessy et al., 1999a; Chiarparin et al., 1999; Pelupessy et al., 1999b; Pang et al., 1999; Reif et al., 2000; Sprangers et al., 2000; Kloiber and Konrat, 2000a,b; Kloiber et al., 2002). On the other hand, preservation of the spin state selectivity in NMR experiments enables effective determination of the various scalar coupling constants in an E.COSY manner (Griesinger et al., 1987; Wagner et al., 1991; Weisemann et al., 1994). The quality of spectra obtained with proteins of larger molecular weight can be significantly improved by the use of TROSY (Pervushin et al., 1997). TROSY is a spectroscopic technique based on the constructive use of interference effects without mixing of the relevant spin states. Thus, all these experiments share the same physical basis and consequently, it is instructive to design a highly optimized experiment unifying

*To whom correspondence should be addressed. E-mail: kopeko@phys.chem.com

these approaches, which enables direct determination of the ψ and ϕ angles in larger proteins by the use of the cross-correlated relaxation rates together with the Karplus-type dependencies of the coupling constants.

In this paper we present a new TROSY-type experiment where backbone ψ and ϕ angles are determined using cross-correlated cross relaxation rates between H^{α}-C^{α} and H^{N}-N dipolar interactions and between H^{α}-C^{α} dipolar interaction and N chemical shift anisotropy (CSA).

Simultaneously, the values of the $^{3,4}J_{H\alpha HN}$ scalar couplings are measured in an E.COSY manner.

In the case of the ϕ angle, the Karplus curve for $^{3}J_{H\alpha HN}$ yields an independent angle determination (Karplus, 1959), whereas $^{4}J_{H\alpha HN}$ might provide additional yet not parametrized constraints on the ψ angle (Vuister and Bax, 1994).

Methods

We introduce two basic variants of the experimental scheme of Figure 1, which are optimized for applications at lower (up to 600 MHz) and higher polarizing magnetic field strength B_0, respectively. In the following, the coherence transfer pathways in each of the two experiments are analyzed using the product operator formalism (Sørensen et al., 1983).

The [^{15}N,^{13}C]-DQ/ZQ-[^{15}N,^{1}H]-TROSY-E. COSY designed for use at lower B_0 omits the double inversion of the $^{1}H^{N}$ spins during MQ evolution making full use of TROSY-type relaxation compensation. To emphasize this fact, the symbol $\overline{\mathrm{H}}$ (= inversion) is added to the corresponding experiment names. The four relevant coherence tranfer pathways are given by Equation 1.

$$\begin{aligned} &H_z \rightarrow MQ\left(\tfrac{E}{2}-H_z^N\right)\left(\tfrac{E}{2}\mp H_z^{\alpha}\right)\exp[-2R_{\beta/\alpha}^{MQ}T_{MQ} \\ &-i(\Omega^{MQ}\mp\pi J_{HC}-\pi J_{HN})t_1] \\ &\rightarrow N_+^{34}\left(\tfrac{E}{2}\mp H_z^{\alpha}\right)\exp[-2R^{34}T_N-i\Omega^{34}t_2] \\ &\rightarrow H_-^{24}\left(\tfrac{E}{2}\mp H_z^{\alpha}\right)\exp[-R^{24}t_3-i\Omega^{24}t_3], \end{aligned} \tag{1}$$

where *MQ* represents either one of the two double-quantum operators (DQ), $C_{\pm}N_{\pm}$, or one of the two zero-quantum operators (ZQ), $C_{\mp}N_{\pm}$, and N_+^{34} and H_-^{24} are the single-transition basis operators $N_+(E/2-H_z)$ and $N_-(E/2+H_z)$, respectively. The chemical shifts relative to the carrier frequencies are $\Omega^{DQ}=\Omega^N+\Omega^C$, $\Omega^{ZQ}=\Omega^N-\Omega^C$, $\Omega^{34}=\Omega^N-\pi J_{HN}$ and $\Omega^{24}=\Omega^H+\pi J_{HN}\cdot J_{HN}$ and J_{HC} are the scalar coupling constants between $^{1}H^{N}$ and ^{15}N spins and between $^{1}H^{\alpha}$ and $^{13}C^{\alpha}$ spins, respectively. R^{34} and R^{24} are the relaxation rates of the corresponding TROSY operators (Pervushin et al., 1997). The MQ relaxation rates $R_{\beta/\alpha}^{MQ}$ are given by Equations 2–5, where the indices α and β correspond to the spin state operators $E/2+H_z^{\alpha}$ and $E/2-H_z^{\alpha}$, respectively (Korzhnev et al., 2001) and only terms proportional to $J(0)$ and $J(\Omega^{H\alpha}-\Omega^{HN})$ are retained:

$$\begin{bmatrix} R_{\beta}^{DQ} \\ R_{\alpha}^{DQ} \\ R_{\beta}^{ZQ} \\ R_{\alpha}^{ZQ} \end{bmatrix} = \begin{bmatrix} 1 & 1-1-1-1-1 & 1 & 0 \\ 1 & 1 & 1-1 & 1-1-1 & 1 \\ 1-1-1-1 & 1 & 1-1 & 0 \\ 1-1 & 1-1-1 & 1 & 1 & 1 \end{bmatrix} \times$$

$$\begin{bmatrix} \frac{8}{3}(A_{CSA(C)}^2+A_{CSA(N)}^2)B_0^2+\frac{2}{3}(A_{D(HC)}^2 \\ +A_{D(HN)}^2)J(0) \\ \frac{16}{3}A_{CSA(C)}A_{CSA(N)}P(\Theta_{CSA(C)CSA(N)}) \\ B_0^2J(0) \\ \frac{8}{3}A_{D(HC)}A_{CSA(C)}P(\Theta_{D(HC)CSA(C)})B_0J(0) \\ \frac{8}{3}A_{D(HN)}A_{CSA(N)}P(\Theta_{D(HN)CSA(N)})B_0J(0) \\ \frac{8}{3}A_{D(HC)}A_{CSA(N)}P(\Theta_{D(HC)CSA(N)})B_0J(0) \\ \frac{8}{3}A_{D(HN)}A_{CSA(C)}P(\Theta_{D(HN)CSA(C)})B_0J(0) \\ \frac{4}{3}A_{D(HC)}A_{D(HN)}P(\Theta_{D(HC)D(HN)})J(0) \\ \frac{2}{3}A_{D(H\alpha HN)}{}^2J(\Omega^{H\alpha}-\Omega^{HN}) \end{bmatrix} \tag{2–5}$$

The spectral density functions $J(\omega)$ of the spectral frequency ω in an approximation of fast internal motions and interaction constants for CSA of nucleus k ($A_{CSA(k)}$) and for dipole-dipole interaction of a given ^{1}H and a nucleus k ($A_{D(Hk)}$) are given by Equations 6–9. In addition we assume that various auto- and cross-correlated relaxation spectral densities encountered in the same spin system can be reasonably represented by the same functional form given by Equation 6.

$$J(\omega)=\frac{\tau_c S^2}{1+\omega^2\tau_c^2}, \tag{6}$$

$$A_{CSA(k)}=-\sqrt{\frac{3}{10}}\frac{1}{2}\gamma k\delta_z^k, \tag{7}$$

$$A_{D(Hk)}=\sqrt{\frac{3}{10}}\frac{\mu_0}{8\pi^2}\gamma k\gamma H^h\left\langle\frac{1}{r_{Hk}^3}\right\rangle, \tag{8}$$

$$P(\Theta)=\frac{3(\cos\Theta)^2-1}{2}, \tag{9}$$

where τ_c is the correlation time, S^2 the generalized order parameter, γ_k the gyromagnetic ratio of the

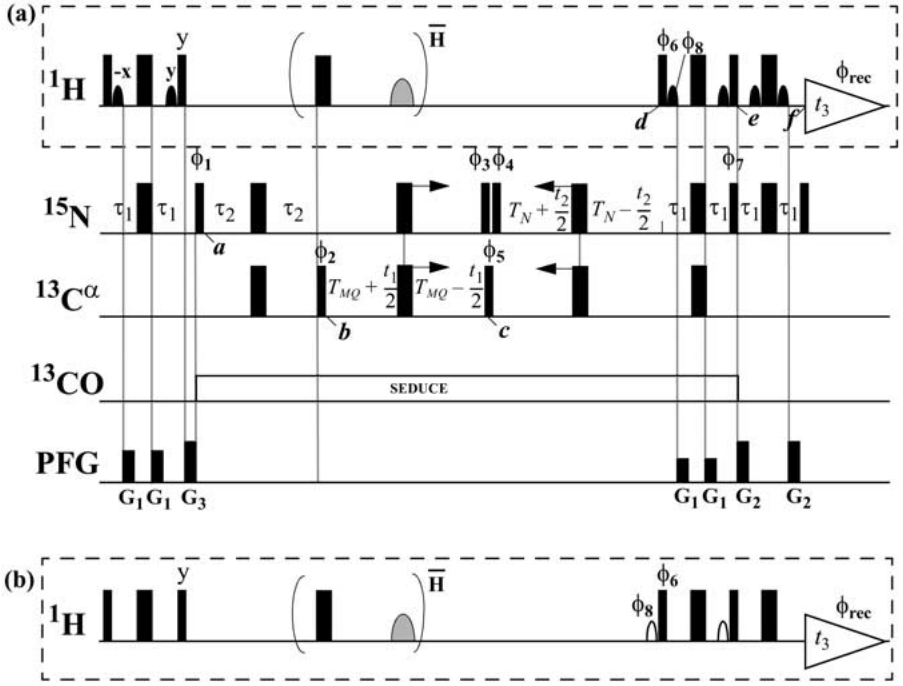

Figure 1. The experimental scheme of the (a) [^{15}N, ^{13}C]-DQ/ZQ-[^{15}N,^{1}H]-TROSY and (b) [^{15}N,^{13}C]-DQ/ZQ- [^{15}N,^{1}H]-TROSY-E. COSY. A variant of each experiment designed for use at polarizing magnetic field strengths Bo higher than 600 MHz (see Methods) is obtained by the insertion of two $^1H^N$ inversion pulses indicated in brackets. Narrow (wide) black bars represent non-selective 90° (180°) pulses on ^{1}H, $^{13}C^\alpha$, ^{15}N and $^{13}C'$ with carrier offsets placed at 4.7 ppm, 55.0 ppm, 118.7 ppm and 175.5 ppm, respectively. Black and open curved shapes indicate selective 90° Gaussian pulses on the water ^{1}H resonance with a duration of 1 ms and selective 90° E-Burp pulses on $^1H^\alpha$ and water ^{1}H with a duration of 1.5 ms, respectively (Geen and Freeman, 1991). The grey curved shapes represent $^1H^N$-selective 180° I-Burp pulses. The boxes on the line labeled PFG indicates sine-shaped pulsed magnetic field gradients along the z-axis with 1 ms duration except for G2 in (b), which has a duration of 950 μs: G1, 30 G cm^{-1}; G2 80 G cm^{-1}; 60 G cm^{-1}. The delays are: $\tau_1 = 2.7$ ms, $\tau_2 = 18$ ms and 34 ms for the determination of the ϕ and ψ angles, respectively, $T_{MQ} = 10.8$ ms, $T_N = \tau_2$ in (a) and $T_N = \tau_2 - \tau_1$ in (b). The 16 separately stored interferograms c_i (i = 1...16) are obtained by the following phases: $\phi_1 = \phi_2 = \{x, x, x, x, x, x, x, x, y, y, y, y, y, y, y, y\}$; $\phi_3 = \{x\}$; $\phi_4 = \{x, x, x, x, -x, -x, -x, -x\}$; $\phi_5 = \{x, y, x, y, x, y, x, y, y, y, -x, y, -x, y, -x, y, -x\}$; $\phi_6 = \phi_7 = \{y, y, -y, -y\}$; $\phi_8 = \{-x, -x, x, x\}$; $\phi_{rec} = \{x, y, x, -y, x, y, x, -y, -y, x, -y, -x, -y, x, -y, -x\}$; x on all pulses without phase specification. The basic 4-step phase cycle is carried out for each of the 16 interferograms in the following manner: $\phi_1 = \{u, -u, -u, u\}$; $\phi_2 = \{u, -u, u, -u\}$; $\phi_{rec} = \{v, v, -v, -v\}$, where u and v stand for x or y. $^{13}C'$ decoupling is performed using the SEDUCE phase modulation (McCoy and Mueller, 1992). Spectra are processed by a linear combination of the obtained set of the interferograms as described in Methods.

nucleus k, δ_z^k the axial principal component of the anti-symmetrical part of the chemical shift tensor for nucleus k, which is assumed to be axially symmetric, μ_0 the permeability of free space, *h* Plancks constant, r_{Hk} the distance between the spins ^{1}H and k, and Θ the projection angle between the indicated interactions (Figure 2).

For glycine residues, a set of equations similar to Equations 2–5 have been derived in closed form. In brief, each the of Equations 2–5 is replaced by two equations corresponding to the up or down state of the second proton directly attached to the C^α atom. In the right hand expression of each modified equation, the terms containing $A_{D(HC)}$ are replaced by two terms corresponding to the spin states of the $^1H^{\alpha 1}$ and $^1H^{\alpha 2}$ spins. In addition, a term describing the $H^{\alpha 1}$-C^α/$H^{\alpha 2}$-C^α dipole/dipole interaction is added.

The initial ^{1}H polarization is transfered by an INEPT step to N_+^{34} at time point a, followed by a pulse segment which creates double- and zero-quantum coherence between ^{15}N and ^{13}C at time point b (Figure 1a). The MQ operators are represented as a linear combination of two single transition operators with respect to the single transitions of the $^1H^N$ and $^1H^\alpha$ spins, $MQ(E/2 - H_z^N)(E/2 - H_z^\alpha$ and $MQ(E/2 - H_z^N)(E/2 + H_z^\alpha)$. During the constant time period T_{MQ} between the time points b and c, these operators evolve due to the MQ chemical shifts Ω^{DQ} and Ω^{ZQ} and the scalar couplings of $^1J_{HN}$ and $^1J_{HC}$. Between time points c and e, the MQ co-

Table 1. The subspectra $\Sigma_1 - \Sigma_{16}$ obtained by linear combination of the interferograms c_1-c_{16} and the resulting spectral terms used to reconstruct phase sensitive 3D [^{15}N,^{13}C]-DQ/ZQ-[^{15}N,^{1}H]-TROSY-E. COSY subspectra

	c1	c2	c3	c4	c5	c6	c7	c8	c9	c10	c11	c12	c13	c14	c15	c16	Spectra terms
Σ1	−	−	−	−	−	+	−	+	−	−	+	+	+	−	−	+	$\cos(\omega^{ZQ}t_1)\sin(\omega^{12}t_2)H^{24}y$
Σ2	+	+	+	+	−	+	−	+	+	+	−	−	+	−	−	+	$\sin(\omega^{ZQ}t_1)\cos(\omega^{12}t_2)H^{24}y$
Σ3	−	−	+	+	+	−	−	−	+	+	+	+	+	−	+	−	$\sin(\omega^{ZQ}t_1)\sin(\omega^{12}t_2)H^{24}x$
Σ4	−	−	+	+	−	+	+	−	−	−	−	−	+	−	+	−	$\cos(\omega^{ZQ}t_1)\cos(\omega^{12}t_2)H^{24}x$
Σ5	−	−	−	−	−	+	−	+	+	+	−	−	−	+	+	−	$\cos(\omega^{DQ}t_1)\sin(\omega^{34}t_2)H^{13}y$
Σ6	+	+	+	+	−	+	−	+	−	−	+	+	−	+	+	−	$\sin(\omega^{DQ}t_1)\cos(\omega^{34}t_2)H^{13}y$
Σ7	+	+	−	−	−	+	+	−	−	−	−	−	−	+	−	+	$\sin(\omega^{DQ}t_1)\sin(\omega^{34}t_2)H^{13}x$
Σ8	+	+	−	−	+	−	−	+	−	−	−	−	+	−	+	−	$\cos(\omega^{DQ}t_1)\cos(\omega^{34}t_2)H^{13}x$
Σ9	−	+	−	+	−	−	−	−	−	+	+	−	+	+	−	−	$\cos(\omega^{DQ}t_1)\sin(\omega^{12}t_2)H^{24}y$
Σ10	+	−	+	−	−	−	−	−	+	−	−	+	+	+	−	−	$\sin(\omega^{DQ}t_1)\cos(\omega^{12}t_2)H^{24}y$
Σ11	−	+	+	−	+	+	+	−	−	+	−	+	−	−	−	−	$\sin(\omega^{DQ}t_1)\sin(\omega^{12}t_2)H^{24}x$
Σ12	−	+	+	−	−	−	+	+	−	+	−	+	+	+	+	+	$\cos(\omega^{DQ}t_1)\cos(\omega^{12}t_2)H^{24}x$
Σ13	−	+	−	+	−	−	−	−	+	−	−	+	−	−	+	+	$\cos(\omega^{ZQ}t_1)\sin(\omega^{34}t_2)H^{13}y$
Σ14	+	−	+	−	−	−	−	−	−	+	+	−	−	−	+	+	$\sin(\omega^{ZQ}t_1)\cos(\omega^{34}t_2)H^{13}y$
Σ15	−	+	+	−	+	+	−	−	+	−	+	−	+	+	+	+	$\sin(\omega^{ZQ}t_1)\sin(\omega^{34}t_2)H^{13}x$
Σ16	+	−	−	+	+	+	−	−	−	+	−	+	+	+	+	+	$\cos(\omega^{ZQ}t_1)\cos(\omega^{34}t_2)H^{13}x$

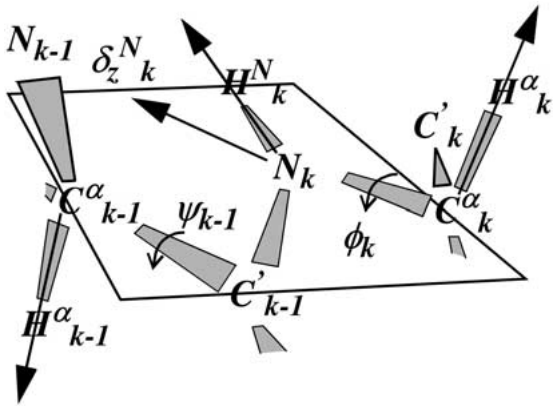

Figure 2. Schematic representation of the protein backbone geometry. The arrows indicate the vectors on which the measured relaxation rates depend. δ_Z^N is the axial principal component of the anti-symmetrical part of the ^{15}N chemical shift tensor, ψ and ϕ are the dihedral angles defining the backbone conformation. Small variations of the ^{15}N chemical shift tensor principal components and thier directions throughout the polypeptide chain can be expected (see for review Pervushin, 2000).

herence is transfered back to the ^{15}N spins via the single-transition TROSY operator N_+^{34} followed by the standard ST2-PT element, which transfers N_+^{34} to H_-^{24} (Pervushin et al., 1998). For the experiment of Figure 1b the $(E/2 - H_z^\alpha)$ and $(E/2 + H_z^\alpha)$ spin states are not mixed during the ST2-PT element, so that the peaks of the resulting doublets (or triplets in the case of glycines) shown in Figure 4 are shifted by $^{3,4}J_{H\alpha HN}$ relative to each other in the Ω^H-dimension. The inclusion of a water-flip-back as implemented in the experimental scheme of Figure 1a, results in partial mixing of the $(E/2 - H_z^\alpha)$ and $(E/2 + H_z^\alpha)$ spin states for $^1H^\alpha$ excited by the selective pulses, which prevents quantitative measurements of the $^{3,4}J_{H\alpha HN}$ coupling constants but not cross correlated relaxation rates. Thus, if sensitivity losses due to the water saturation is not a question, the water flip back trick should be avoided.

In order to maximize the spectral sensitivity, all coherence transfer pathways are retained. The individual phase sensitive subspectra such as the 3D TROSY-ZQ-HNCA and the 3D TROSY-DQ-HNCA are then obtained from linear combinations of 16 separately stored interferograms measured for each (t_1, t_2)-pair (Figure 1). Table 1 summarizes the linear combinations employed to obtain each subspectrum. In Table 1 the column c_i represents the sign of the contribution of the i-th interferogram given in Figure 1 to the j-th subspectrum Σ_j, where both i and j range from 1 to 16. The complex exponents $\exp(-\Omega^{MQ}t_1)\exp(-\Omega^{12/34}t_2)$ required for the complex Fourier transformation are obtained by combining four of the cosine and sine modulated terms. For example, $\exp(-\Omega^{MQ}t_1)\exp(-\Omega^{12/34}t_2)$ is built up with the subspectra Σ_5-Σ_8. Finally, only spectra showing the slowly relaxing TROSY components

in the [^{1}H,^{15}N]-plane (Pervushin et al., 1997) are retained for further analysis. Neglecting transverse relaxation one quarter of the initially combined $^1H^N$ and ^{15}N Boltzmann steady state magnetizations contribute to the individual TROSY-DQ-HNCA or TROSY-ZQ-HNCA spectra. The losses stem from the TROSY selection and the States-TPPI quadrature detection of the MQ frequencies.

In order to obtain structural information, the four relaxation rates of the doublet peaks in the DQ- and ZQ-spectra are linearly combined resulting in cancelation of all terms except for the dipole(HC)/dipole(HN) and dipole(HC)/CSA(N)-cross-correlated terms given by Equation 10.

$$[A_{D(C)}A_{D(N)}P(\Theta_{D(C)D(N)}) - 2A_{D(C)}A_{CSA(N)}B_0 P(\Theta_{D(C)CSA(N)})]\tfrac{4}{3}J(0) = (R_\beta^{DQ} - R_\alpha^{DQ} - R_\beta^{ZQ} + R_\alpha^{ZQ})\tfrac{1}{4}. \quad (10)$$

To be able to derive the expressions for the ψ and ϕ angles in a closed form, we further assume that the difference in contribution of the passive scalar couplings to ZQ and DQ coherences is neglegible. In that case, the linear combination of the relaxation rates on the right side of Equation 10 can be expressed via the experimentally measured intensities of the 3D cross-peaks in the DQ and ZQ spectra:

$$(R_\beta^{DQ} - R_\alpha^{DQ} - R_\beta^{ZQ} + R_\alpha^{ZQ})\tfrac{1}{4} = \frac{1}{T_{MQ}} \ln \frac{I_\alpha^{DQ} I_\beta^{ZQ}}{I_\beta^{DQ} I_\alpha^{ZQ}}. \quad (11)$$

A combination of (10) and (11) yields:

$$[A_{D(C)}A_{D(N)}P(\Theta_{D(C)D(N)}) - 2A_{D(C)}A_{CSA(N)}B_0 P(\Theta_{D(C)CSA(N)})]\tfrac{4}{3}J(0) = \frac{1}{T_{MQ}} \ln \frac{I_\alpha^{DQ} I_\beta^{ZQ}}{I_\beta^{DQ} I_\alpha^{ZQ}}, \quad (12)$$

which indicates the relationship between the intensities of the MQ peak components and the projection angles resulting from cross-correlated relaxation of both the dipole-dipole and dipole-CSA interactions involving Cα and N spins.

A similar relationship for Gly residues is provided by Equation 13, where only the outer components of the MQ triplets corresponding to both $^1H^{\alpha 1}$ and $^1H^{\alpha 2}$ spins in αα or ββ state are used.

$$[A_{D(C)}A_{D(N)}(P(\Theta^1_{D(C)D(N)}) + P(\Theta^2_{D(C)D(N)})) - 2A_{D(C)}A_{CSA(N)}B_0(P(\Theta^1_{D(C)CSA(N)}) + P(\Theta^2_{D(C)CSA(N)}))]\tfrac{4}{3}J(0) = \frac{1}{T_{MQ}} \ln \frac{I_{\alpha\alpha}^{DQ} I_{\beta\beta}^{ZQ}}{I_{\beta\beta}^{DQ} I_{\alpha\alpha}^{ZQ}}. \quad (13)$$

All elements of the described experiment are optimized for TROSY relaxation. A graphical representation of Equations 12 and 13 given by Figure 3 shows

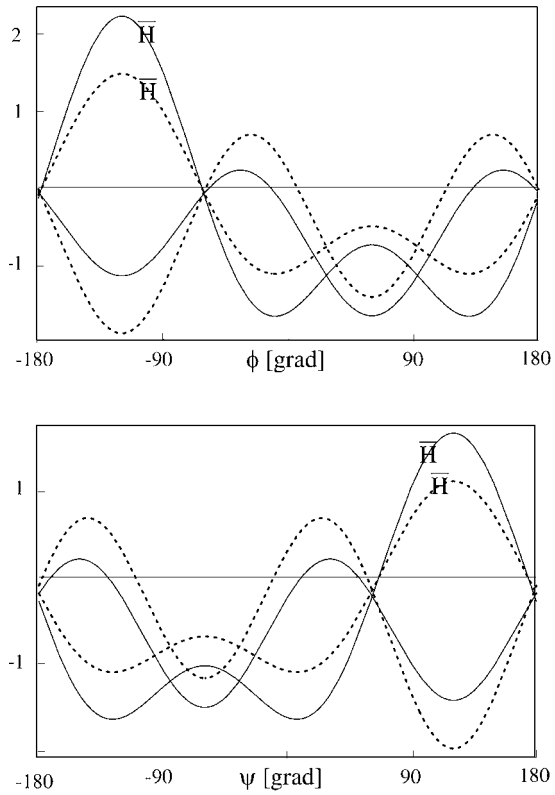

Figure 3. The left-hand sides of Equations 12 and 14 as functions F of the dihedral ϕ and ψ angles at 900 MHz (solid curves) and 600 MHz (broken curves) fields. The assumptions mentioned in the Results part are made. The modification $\overline{H}$ yields a doubled variation of the relaxation rates.

that the most effective use of the experiment can be achieved at polarizing magnetic fields up to 600 MHz. Since the second terms on the left side of both Equations 12 and 13 depend linearly on B_0, the right side becomes smaller at higher fields. To circumvent this reduction, we propose the use of the same experimental scheme supplemented with $\overline{H}$. Due to the interchange of the single-transition operators in the middle of the MQ-evolution period the relaxation term describing the dipole(HC)/dipole(HN) cross-correlation is canceled out, whereas the term stemming from the dipole(HC)/CSA(N) cross-correlation remains unchanged as it is described by Equations 14 and 15.

$$-2A_{D(C)}A_{CSA(N)}B_0 P(\Theta_{D(C)CSA(N)})\tfrac{4}{3}J(0) = \frac{1}{T_{MQ}} \ln \frac{I_\alpha^{DQ} I_\beta^{ZQ}}{I_\beta^{DQ} I_\alpha^{ZQ}}, \quad (14)$$

$$-2A_{D(C)}A_{CSA(N)}B_0 P(\Theta^1_{D(C)CSA(N)}) + P(\Theta^2_{D(C)CSA(N)}))\tfrac{4}{3}J(0) = \frac{1}{T_{MQ}} \ln \frac{I_{\alpha\alpha}^{DQ} I_{\beta\beta}^{ZQ}}{I_{\beta\beta}^{DQ} I_{\alpha\alpha}^{ZQ}}. \quad (15)$$

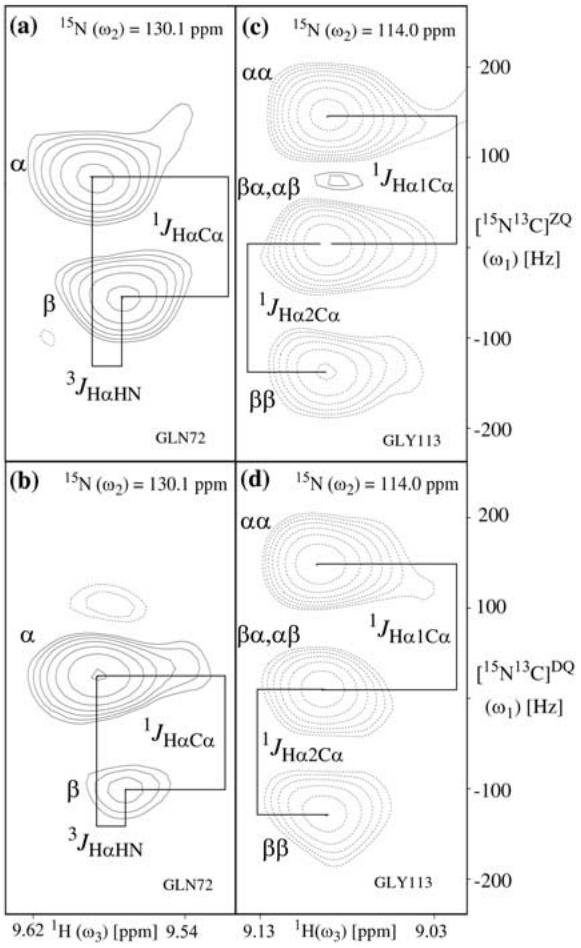

Figure 4. [^{1}H,^{15}N/^{13}C-MQ] planes of selected cross-peaks from the 3D [^{15}N,^{13}C]-DQ/ZQ-[^{15}N,^{1}H]-TROSY-E. COSY spectra of a sample of ^{15}N/^{13}C-labeled apo-CcmE30-159-H6 (Enggist et al., 2002, accepted) used for the ϕ angle determination. Spectra of the experiment employing selective 90° E-Burp pulses with $\overline{H}$ are shown in (a) and (b). The peak doublets of Gln72 result from the $J_{H\alpha C\alpha}$ splitting in the ω_{MQ} dimension. Due to the E. COSY effect the peaks are shifted in the ω_H dimension by $^3J_{H\alpha HN} = 9.3$ Hz and $^3J_{H\alpha HN} = 8.2$ Hz in (a) and (b), respectively. Spectra of the experiment using selective 90° Gaussian pulses without $\overline{H}$ are shown in (c) and (d). The peak triplet of Gly113 results from the $J_{H\alpha1C\alpha}$ and $J_{H\alpha2C\alpha}$ splittings in the ω_{MQ} dimension. For the relaxation calculations the intensities of the outer peaks corresponding to the αα and ββ states are used. The inner peaks are superpositions of the peaks corresponding to the βα and αβ states. The experiments were performed on a Bruker *Avance* 600 MHz spectrometer. The 16 complex interferograms consisting of 60 × 30 × 512 data points along the ω_1, ω_2 and ω_3 dimensions are collected and processed with PROSA (Güntert et al., 1992) as described in Methods. The experiments using selective Gaussian pulses (E-Burp pulses) were acquired with an interscan delay of 850 ms (800 ms) and 16 (4) scans per datapoint resulting in a total acquisition time of 130 (31) hours. (e) shows 1D [^{15}N^{13}C]ZQ (ω_1) slices taken at the positions of the maximum intensity of the cross-peaks in (a) to demonstrate the quality of the acquired spectra.

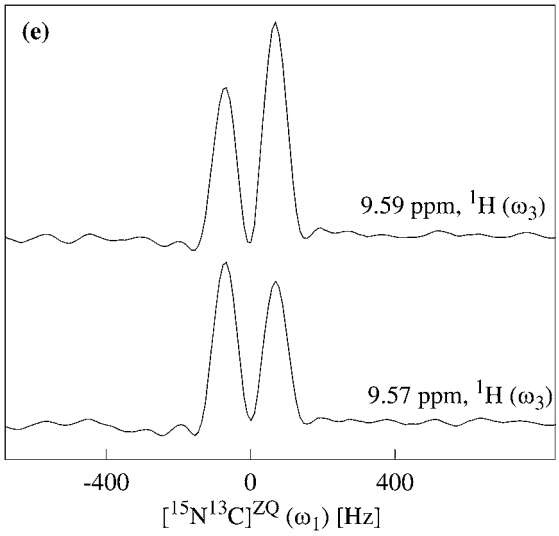

Figure 4. Continued.

The right-hand sides of Equations 12 and 14 are compared as functions F of the dihedral angles ϕ and ψ at 600 MHz (dotted curves) and 900 MHz ^{1}H fields (solid curves) in Figure 3. The double inversion of $^1H^N$ at 900 MHz achieved in the experimental scheme of Figure 1 results in a twofold increase in the range of relaxation rates observed for different dihedral angles in comparison with the full TROSY version. In addition, the redundancy of possible dihedral angles deduced from the relaxation rates is reduced to two from four possible angles. Pure dipole(HC)/dipole(HN) crosscorrelated relaxation terms can be obtained by subtracting Equation 14 from Equations 12 and 15 from Equation 13, respectively, whereas $\overline{H}$ increases the amplitude of the variation of the relaxation rates measured at 900 MHz fields. No such benefit is derived at 600 MHz fields so that $\overline{H}$ can be omitted.

Results and discussion

The experimental schemes of Figure 1 were applied to the 16 kDa uniformly ^{13}C, ^{15}N labeled cytochrome *c* maturation heme chaperone protein E from *E. coli* (CcmE). The NMR sample contained 350 µl of 1 mM protein solution in 20 mM sodium phosphate buffer at pH = 6.0 containing in addition 300 mM NaCl. The CcmE family of proteins exhibits no significant amino acid sequence homology to any protein of a known 3D structure (Enggist et al., 2002, accepted). The high resolution 3D structure of CcmE determined by solution NMR techniques (PDB code 1LIZ) serves as a

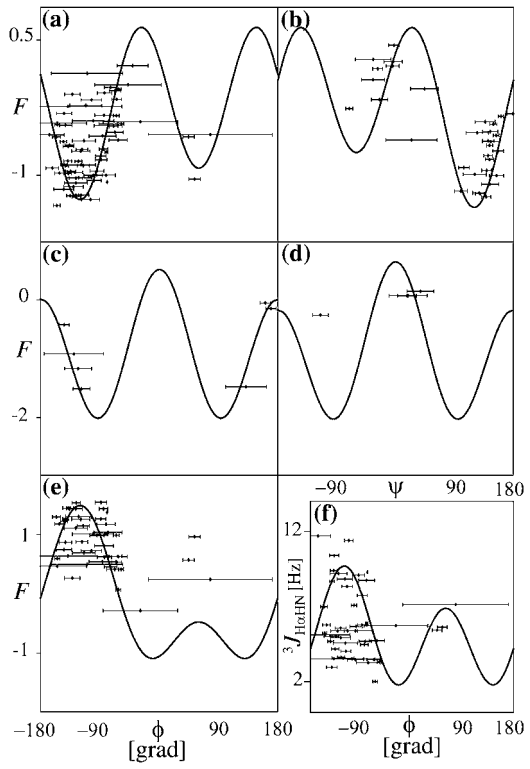

Figure 5. Experimental values of $F = \ln\left(I^{DQ}_{\alpha(\alpha)} I^{ZQ}_{\beta(\beta)} \Big/ I^{DQ}_{\beta(\beta)} I^{ZQ}_{\alpha(\alpha)}\right)$ measured at $B_0 = 600$ MHz vs. mean angles derived from the set of the 20 conformers representing the solution structure of CcmE (Enggist et al., 2002, accepted). (a) F vs. ϕ or all amino acids except for Gly, (b) F vs. ψ for all amino acids except for Gly, (c) F vs. ϕ for Gly, (d) F vs. ψ for Gly, (e) F vs. ϕ for all amino acids except for Gly with $\overline{H}$ (see Methods section), (f) $^3J_{H\alpha HN}$ vs. ϕ. The solid curves represent theoretical values. The error bars show the distribution of the angle within the 20 NMR conformers.

representative for this class of proteins. ^{15}N relaxation rates were used to estimate the product of the averaged generalized order parameter and the rotational correlation time of the protein, $\tau_c S^2 = 10 \pm 1$ ns (Enggist et al., 2002, accepted).

In order to maximize the spectral sensitivity and facilitate data evaluation, the experiments of Figure 1 were run separately for the ϕ_k and ψ_{k-1} angle estimations using either $\tau_2 = 18$ ms or $\tau_2 = 34$ ms yielding mostly transfer from $^{15}N_k$ to $^{13}C^{\alpha}_k$ or $^{15}N_k$ to $^{13}C^{\alpha}_{k-1}$, respectively. Figure 2 shows the geometry of a fragment of the polypeptide backbone with the nomenclature indicated for atoms and angles involved in the analysis. We assume that for any given polypeptide fragment relaxation of the corresponding multiple quantum coherences excited between the $^{15}N_k$ and $^{13}C^{\alpha}_{k-1}$ and $^{15}N_k$ and $^{13}C^{\alpha}_{k-1}$ spins depends only on the values of the ϕ_k and ψ_{k-1} angles. The following projection angles and distances were assumed to be identical for all peptide groups: H^{α}_k-$C^{\alpha}_k = 108.4°$ and $H^{\alpha 1/2}_k - C^{\alpha}_k - N_k = 111°$ for glycines, $H^{N}_k - N_k - C^{\alpha}_k = 116°$, $C^{\alpha}_{k-1} - C'_{k-1} - N_k = 116°$, $C'_{k-1} - N_k - H^{N}_k = 116,5°$, $H^{\alpha}_k - C^{\alpha}_k - C'_k = 107.2°$, $r_{HN} = 1.04 \times 10^{10}$ m (Roberts et al., 1987), $r_{HC} = 1.09 \times 10^{10}$ m (Case, 1999). The main axis of the ^{15}N CSA tensor is located in the peptide plane deviating from the HN bond by 20° (Oas et al., 1987) with the main eigenvalue $\Delta\delta(^{15}N\ CSA) = 170$ ppm (Tjandra et al., 1996). The dihedral angles ϕ_k and ψ_{k-1} are related to the projection angles between the interactions by geometrical considerations. The ratios of the MQ relaxation rates as functions of the ϕ and ψ angles are listed in the Tables 2a-c. The functions are given in units of $S^2\tau_c \times 10^8\ s^{-1}$ and therefore are independent of τ_c. The Tables 2a and 2b show the functions of Equations 12–15 calculated for $B_0 = 600$ MHz without and with $\overline{H}$. Table 2c reports the corresponding functions for $B_0 = 900$ MHz, where H is important due to the significantly reduced strength of the combined HC/HN dipole/dipole and HC/N dipole/CSA interactions observed in TROSY spectra recorded without $\overline{H}$.

The logarithms of the ratio of the measured MQ relaxation rates, $F = \ln\left(I^{DQ}_{\alpha(\alpha)} I^{ZQ}_{\beta(\beta)} \Big/ I^{DQ}_{\beta(\beta)} I^{ZQ}_{\alpha(\alpha)}\right)$, for the ϕ and ψ angles were obtained from the 3D [^{15}N,^{13}C]-DQ/ZQ-[^{15}N,^{1}H]-TROSY-E.COSY spectra. In the $\overline{H}$ experiment, both the ratio of the relaxation rates and the experimental $^3J_{H\alpha HN}$ scalar coupling constants are extracted from the same data set measured with the experimental scheme of Figures 2b. Figures 4a and 4b show the 2D doublet corresponding to the backbone moiety of Gln72 measured with the experiment [^{15}N,^{13}C]-DQ/ZQ-[^{15}N,^{1}H]-TROSY-E.COSY-H in the ZQ- and DQ-spectra, respectively. An example of a glycine 2D triplet is given in Figures 4c and 4d. The 2D triplet of Gly113 is obtained from the [^{15}N,^{13}C]-DQ/ZQ-[^{15}N,^{1}H]-TROSY-E.COSY experiment.

Figures 5a–e show the logarithms of the ratio of the measured MQ relaxation rates, F, versus the values of the ϕ angles averaged over 20 NMR conformers of the structurally well defined core of CcmE (residues 34–132) along with the theoretical curves calculated with Equations 12–15.

In general, a satisfactory correlation between the experimental relaxation data and the angle values cal-

Table 2. Logarithm of the ratio of peak amplitudes in 3D [^{15}N,^{13}C]-DQ/ZQ-[^{15}N,^{1}H]-TROSY-E. COSY subspectra as a function of the ϕ and ψ dihedral angles measured at $B_0 = 600$ MHz (a and b) and $B_0 = 900$ Mhz (c). The functions in (a) correspond to the experimental scheme of Figure 1 applied without $\overline{H}$ and the functions in (b) and (c) correspond to the scheme applied with $\overline{H}$ during DQ and ZQ evolution

(a)	$\ln\left(\frac{I^{DQ}_{\alpha(\alpha)} I^{ZQ}_{\beta(\beta)}}{I^{DQ}_{\beta(\beta)} I^{ZQ}_{\alpha(\alpha)}}\right)[\tau_c \times 10^8]\,s^{-1}$
ϕ	$0.696 + 0.234\cos(\phi - 60) - 2.327\cos^2(\phi - 60)$
ψ	$0.677 + 0.410\cos(\psi - 120) - 2.252\cos^2(\psi - 120)$
ϕ_{Gly}	$1.416 + 0.251\cos(\phi - 60) - 2.283\cos^2(\phi - 60) + 0.251\cos(\phi + 60) - 2.283\cos^2(\phi + 60)$
ψ_{Gly}	$1.354 + 0.410\cos(\psi - 120) - 2.252\cos^2(\psi - 120) + 0.410\cos(\psi + 120) - 2.252\cos^2(\psi + 120)$
(b)	
ϕ	$-0.927 + 0.985\cos(\phi - 60) + 1.429\cos^2(\phi - 60)$
ψ	$-0.918 + 0.902\cos(\psi - 120) + 1.138\cos^2(\psi - 120)$
ϕ_{Gly}	$-1.795 + 1.057\cos(\phi - 60) - 1.402\cos^2(\phi - 60) - 1.057\cos(\phi + 60) + 1.402\cos^2(\phi + 60)$
ψ_{Gly}	$-1.836 + 0.902\cos(\psi - 120) + 1.138\cos^2(\psi - 120) + 0.902\cos(\psi + 120) + 1.138\cos^2(\psi + 120)$
(c)	
ϕ	$-1.390 - 1.477\cos(\phi - 60) + 2.144\cos^2(\phi - 60)$
ψ	$-1.377 + 1.352\cos(\psi - 120) + 1.707\cos^2(\psi - 120)$
ϕ_{Gly}	$-2.692 - 1.585\cos(\phi - 60) + 2.103\cos^2(\phi - 60) - 1.585\cos(\phi + 60) + 2.103\cos^2(\phi + 60)$
ψ_{Gly}	$-2.754 + 1.352\cos(\psi - 120) + 1.707\cos^2(\psi - 120) + 1.352\cos(\psi + 120) + 1.707\cos^2(\psi + 120)$

culated from the NMR structure of CcmE is observed. The error propagation of the signal to noise ratio in the [^{15}N,^{13}C]-DQ/ZQ-[^{15}N,^{1}H]-TROSY-E.COSY spectra used to estimate the ϕ angles typically yields an error of 6% for the F values. Statistically significant deviations of the experimental values of F from the theoretical curves of Equations 12–15 are attributed to an absence of traditional structural constraints which restrain the corresponding ϕ and ψ angles in the process of NMR structure calculations. This situation was detected for the ϕ angle of the residues 40, 44, 56, 58, 70, 76, 78, 88, 109, 120, 128, 134, 135 and 142 and for the ψ angle of the residues 45, 55, 61, 70, 81, 88, 102, 110, 113, 119 and 126. Structural refinement using cross-correlated relaxation data serves as a useful complementary tool to the conventional NOEs based constraints in loop regions of the protein structure (Sprangers et al., 2000).

The values of the $^{3,4}J_{H\alpha HN}$ can be independently obtained from both ZQ- and DQ- subspectra of the [^{15}N,^{13}C]-DQ/ZQ-[^{15}N,^{1}H]-TROSY-E. COSY experiment. This fact can be used to reduce the effects of spectral artifacts or peak overlap and in order to calculate statistical uncertainties. In the case of glycine, only the sum of $^{3,4}J_{H\alpha 1HN}$ and $^{3,4}J_{H\alpha 2HN}$ can be measured, since the inner peak of the triplet is a superposition of the peaks corresponding to the $\alpha\beta$ and $\beta\alpha$ states slightly shifted relatively to each one another by $2 \times (^{3,4}J_{H\alpha 1HN} - {}^{3,4}J_{H\alpha 2HN})$. The values of the $^{3}J_{H\alpha HN}$ coupling constants are usually analysed solely as a function of the ϕ angle using the Karplus-type dependencies while a structural parametrization for the $^{4}J_{H\alpha HN}$ coupling constants is not yet available (Vuister and Bax, 1994). Figure 5f correlates measured $^{3}J_{H\alpha HN}$ scalar coupling constants with the theoretical Karplus-type curve (Wüthrich, 1986). Due to transverse relaxation of the $^{1}H^{\alpha}$ spins in the ST2-PT element, the apparant values of the $^{3,4}J_{H\alpha HN}$ scalar couplings smaller than 2 Hz are significantly biased by cross-talk between the α and β states of the $^{1}H^{\alpha}$ spin (Wang and Bax, 1996). As a result only $^{3}J_{H\alpha HN}$ scalar couplings stronger than 3 Hz match well with the angular restraints derived from the relaxation data. We attempted to minimize mixing of the α and β states of the $^{1}H^{\alpha}$ spin in the ST2-PT by introducing $^{1}H^{\alpha}$ band selective 90° pulses, which in combination with the subsequent non-selective 90° ^{1}H hard pulses quantitatively flip the $^{1}H^{\alpha}$ magnetization to the +z axis (Figure 1b). Nonetheless, the experimental values of the scalar coupling constants smaller than 2–4 Hz tend to

be systematically underestimated. With the increased transverse relaxation of $^1H^\alpha$ spins usually found in larger proteins, the systematic errors stemming from the cross-talk problem result in an underestimation of even larger scalar couplings. The positive and negative values of the ϕ angles can be most effectively discriminated by combining cross correlated relaxation rates obtained from the [^{15}N,^{13}C]-DQ/ZQ-[^{15}N,^{1}H]-TROSY-E. COSY experiment run with and without the $\overline{H}$ element (see Figures 3 and 5e). The obtained values of the ϕ angles can be than cross validated using the $^3J_{H\alpha HN}$ scalar coupling constants.

Thus, the TROSY principle has been introduced into a modified MQ-E. COSY-HNCA experiment designed for measurements of the intraresidual and sequential H^α-C^α/H^N-N dipole/dipole and H^α-C^α/N dipole/CSA cross-correlated relaxation rates, which in addition provides values of the $^{3,4}J_{H\alpha HN}$ coupling constants measured in an E. COSY manner. The restraints for backbone ψ and ϕ angles are derived from a ratio of the relaxation rates of ZQ and DQ coherences excited between the $^{13}C^\alpha$ and ^{15}N spins and the Karplus-type dependencies of the coupling constants measured from the corresponding $^1H^\alpha$ spin state selective [^{15}N,^{13}C]-DQ/ZQ-[^{15}N,^{1}H]-TROSY-E. COSY spectra reconstructed from a single data set. A comparison of the measured values of the ψ and ϕ angles of the 16 kDa CcmE protein with the average values determined from the NMR solution structure by traditional methods reveals an overall match between directly measured ψ and ϕ angles with the corresponding angles found in the set of 20 NMR conformers.

We conclude that the values of dihedral angles calculated from the relaxation data are more reliable than the ones derived from the scalar coupling alone. In addition, the comparison indicates a necessity to refine NMR structures by including cross-correlated relaxation-based constraints in structure determination protocol.

Acknowledgements

We thank Dr Fred Damberger for careful reading of the manuscript. We are grateful to Dr Elisabeth Engist and Prof Linda Thony-Meier for the CCME sample. This work was supported by an ETH internal grant to K.P.

Appendix A

The relaxation rate during t_1 is calculated for the four-spin system H^C-C-N-H^N using the following basis in the master equation (Abragam, 1961):

$$\begin{bmatrix} ZQ_1 \\ ZQ_2 \\ ZQ_3 \\ ZQ_4 \\ ZQ_5 \\ ZQ_6 \\ ZQ_7 \\ ZQ_8 \\ DQ_1 \\ DQ_2 \\ DQ_3 \\ DQ_4 \\ DQ_5 \\ DQ_6 \\ DQ_7 \\ DQ_8 \end{bmatrix} = \begin{bmatrix} C_-N_+(E-2H_z^C)(E-2H_z^N) \\ C_+N_-(E-2H_z^C)(E-2H_z^N) \\ C_-N_+(E+2H_z^C)(E-2H_z^N) \\ C_+N_-(E+2H_z^C)(E-2H_z^N) \\ C_-N_+(E-2H_z^C)(E+2H_z^N) \\ C_+N_-(E-2H_z^C)(E+2H_z^N) \\ C_-N_+(E+2H_z^C)(E+2H_z^N) \\ C_+N_-(E+2H_z^C)(E+2H_z^N) \\ C_+N_+(E-2H_z^C)(E-2H_z^N) \\ C_-N_-(E-2H_z^C)(E-2H_z^N) \\ C_+N_+(E+2H_z^C)(E-2H_z^N) \\ C_-N_-(E+2H_z^C)(E-2H_z^N) \\ C_+N_+(E-2H_z^C)(E+2H_z^N) \\ C_-N_-(E-2H_z^C)(E+2H_z^N) \\ C_+N_+(E+2H_z^C)(E+2H_z^N) \\ C_-N_-(E+2H_z^C)(E+2H_z^N) \end{bmatrix}.$$

The relaxation matrix has a pure diagonal form. The DD interactions of the H^α-C^α, H^N-N, N-C^α and H^N-H^α spin pairs, the CSA of the H^α, C, N and H^N spins, and all cross-correlation terms are taken into account. In the slow tumbling regime we retain terms in $J(0)$ only, the exception are terms in the difference and sum of two proton frequencies.

References

Abragam, A. (1961) *The Principles of Nuclear Magnetism*, Clarendon Press, Oxford.
Case, D.A. (1999) *J. Biomol. NMR*, **15**, 95–102.
Chiarparin, E., Pelupessy, P., Ghose, R. and Bodenhausen, G. (1999) *J. Am. Chem. Soc.*, **121**, 6876–6883.
Ernst, M. and Ernst, R.R. (1994) *J. Magn. Reson. Ser.*, **A110**, 202–213.
Geen, H. and Freeman, R. (1991) *J. Magn. Reson.*, **93**, 93–141.
Griesinger, C., Sorensen, O.W. and Ernst, R.R. (1987) *J. Magn. Reson.*, **75**, 474–492.
Güntert, P., Dotsch, V., Wider, G. and Wüthrich, K. (1992) *J. Biomol. NMR*, **2**, 619–629.
Karplus, M. (1959) *J. Chem. Phys.*, **30**, 11–15.
Kloiber, K. and Konrat, R. (2000a) *J. Biomol. NMR*, **17**, 265–268.
Kloiber, K. and Konrat, R. (2000b) *J. Am. Chem. Soc.*, **122**, 12033–12034.
Kloiber, K., Schuler, W. and Konrat, R. (2002) *J. Biomol. NMR*, **22**, 349–363.
Korzhnev, D.M., Billeter, M., Arseniev, A.S. and Orekhov, V.Y. (2001) *Prog. Nucl. Magn. Reson. Spectrosc.*, **38**, 197–266.
McCoy, M.A. and Mueller, L. (1992) *J. Am. Chem. Soc.*, **114**, 2108–2112.

Oas, T.G., Hartzell, C.J., Dahlquist, F.W. and Drobny, G.P. (1987) *J. Am. Chem. Soc.*, **109**, 5962–5966.

Pang, Y.X., Wang, L.C., Pellecchia, M., Kurochkin, A.V. and Zuiderweg, E.R.P. (1999) *J. Biomol. NMR*, **14**, 297–306.

Pelupessy, P., Chiarparin, E., Ghose, R. and Bodenhausen, G. (1999a) *J. Biomol. NMR*, **13**, 375–380.

Pelupessy, P., Chiarparin, E., Ghose, R. and Bodenhausen, G. (1999b) *J. Biomol. NMR*, **14**, 277–280.

Pervushin, K. (2000) *Quart. Rev. Biophys*, **33**, 161–197.

Pervushin, K., Riek, R., Wider, G. and Wüthrich, K. (1997) *Proc. Natl. Acad. Sci. USA*, **94**, 12366–12371.

Pervushin, K., Wider, G. and Wüthrich, K. (1998) *J. Biomol. NMR*, **12**, 345–348.

Reif, B., Diener, A., Hennig, M., Maurer, M. and Griesinger, C. (2000) *J. Magn. Reson.*, **143**, 45–68.

Reif, B., Hennig, M. and Griesinger, C. (1997) *Science*, **276**, 1230–1233.

Roberts, J.E., Harbison, G.S., Munowitz, M.G., Herzfeld, J. and Griffin, R.G. (1987) *J. Am. Chem. Soc.*, **109**, 4163–4169.

Sørensen, O.W., Eich, G.W., Levitt, M.H., Bodenhausen, G. and Ernst, R.R. (1983) *Prog. Nucl. Magn. Reson. Spectrosc.*, **16**, 163–192.

Sprangers, R., Bottomley, M.J., Linge, J.P., Schultz, J., Nilges, M. and Sattler, M. (2000) *J. Biomol. NMR*, **16**, 47–58.

Tjandra, N., Szabo, A. and Bax, A. (1996) *J. Am. Chem. Soc.*, **118**, 6986–6991.

Vincent, S.J.F., Zwahlen, C., Bolton, P.H., Logan, T.M. and Bodenhausen, G. (1996) *J. Am. Chem. Soc.*, **118**, 3531–3532.

Vuister, G.W. and Bax, A. (1994) *J. Biomol. NMR*, **4**, 193–200.

Wagner, G., Schmieder, P. and Thanabal, V. (1991) *J. Magn. Reson.*, **93**, 436–440.

Wang, A.C. and Bax, A. (1996) *J. Am. Chem. Soc.*, **118**, 2483–2494.

Weisemann, R., Ruterjans, H., Schwalbe, H., Schleucher, J., Bermel, W. and Griesinger, C. (1994) *J. Biomol. NMR*, **4**, 231–240.

Wüthrich, K. (1986) *NMR of Proteins and Nucleic Acids*, Wiley, New York, NY.

Yang, D.W. and Kay, L.E. (1998) *J. Am. Chem. Soc.*, **120**, 9880–9887.

Yang, D.W., Gardner, K.H. and Kay, L.E. (1998) *J. Biomol. NMR*, **11**, 213–220.

Yang, D.W., Konrat, R. and Kay, L.E. (1997) *J. Am. Chem. Soc.*, **119**, 11938–11940.